Multi-scale Modelling and Simulation of Material Removal Characteristics in Computer-controlled Bonnet Polishing

Zhong-Chen Cao and Chi Fai Cheung*

Partner State Key Laboratory of Ultra-precision Machining Technology, Department of Industrial and Systems Engineering, The Hong Kong Polytechnic University

* Corresponding author.

Abstract

Computer-controlled Bonnet Polishing (CCBP) is an enabling technology which is capable of fabricating ultra-precision freeform surfaces with sub-micrometer form accuracy and surface roughness in the nanometer range, especially for difficult-to-machine and ferrous materials. However, the material removal mechanism of computer controlled bonnet polishing (CCBP) usually exhibits multidisciplinary and multi-scale complexity and hence our understanding of the material removal characteristics is still far from complete. As a result, this paper presents a multi-scale theoretical model for the prediction and simulation of the material removal characteristics in the CCBP process. The model is established based on the study of contact mechanics, kinematics theory and wear mechanisms. A series of spot polishing tests as well as simulation experiments by the theoretical model were conducted. The predicted results agree well with the experimental data. The successful development of the theoretical model helps to make the CCBP process more predictive, and so that optimizing the manufacturing process, and forms the theoretical basis for explaining some material removal mechanisms in CCUP, such as the critical polishing depth for minimizing pad scratching.

***Keywords**:* Ultra-precision Machining, Bonnet Polishing, Material Removal Characteristics, Multi-scale Modelling, Contact Mechanics

1. Introduction

Free-form surfaces with high form accuracy and good surface finish have become increasingly required for example in the field of precision optical applications [1, 2]. However, the geometrical complexity and high quality requirement of freeform surfaces bring considerable challenges for the fabrication of these surfaces [3]. Computer-controlled Bonnet Polishing (CCBP) is an enabling technology that actively controls the position and orientation of a spinning, inflated, membrane tool

(the 'bonnet') as it sweeps through the polished surfaces [4, 5]. CCBP has the advantage of high polishing efficiency, mathematically tractable influence function, and flexibly controllable spot size with variable tool hardness [6]. Therefore, CCBP is one of the promising ultra-precision polishing technology which shows a great potential with regard to the application value in the fabrication of freeform surfaces with sub-micrometer form accuracy and nanometric surface finish. It is well known that the surface generation of the polishing process can be regarded as the convolution of the influence function and the dwell time map along the pre-specific tool path. Hence a predictable and stable tool influence function and an optimized path generator are of paramount importance for the success of the freeform polishing process. Moreover, polishing of freeform surfaces with submicrometre form accuracy and surface finish in the nanaometric range is complex and multi-scale in nature. As a result, knowledge of the removal mechanisms and factors affecting material removal characteristics are vital to determine the surface quality and form control in the polishing process.

During the past few decades, much research has been performed on the modelling of the material removal characteristics based on the Preston's equation [7-10]. Cheung et al. [11] established a predicted model for the material removal characteristics with the assumption of modified Gaussian distribution of the contact pressure in bonnet polishing. Li et al. [12, 13] and Wang et al. [14] calculated the pressure distribution in the contact area by the axisymmetric elastic solid model with finite element analysis (FEA). However, in their model, the pressure on the polished surface is only related to the elastic deformation of the polishing tool. Bouvier [15] and Zeng et al. [16] developed the material removal model using modified Preston equation and Hertz contact mechanics theory. But the pressure distribution and surface deformation predicted by Hertz's equations must be modified, when comes to that a slurry film is present and the polishing pad slides over the surface in the actual polishing process. Moreover, the material removal characteristics in bonnet polishing is affected by various parameters (tool radius, *precess* angle, polishing depth, head speed, tool pressure, polishing time, polishing cloth, slurry concentration, particle size and type etc.), while the predicted model based on the Preston's equation is only concerned with the velocity of polishing tool relative to the workpiece and the contact pressure between the polishing tool and the workpiece.

Besides the mechanical model based on the Preston's equation, many researchers have developed comprehensive material removal models in order to reveal insights into the contact behavior and wear mechanism in the similar chemical-mechanical polishing (CMP) process. Luo and Dornfeld [17] developed an indentation-sliding model for predicting the material removal rate with the fully plastic deformation assumption over the wafer–abrasive interface. In their model, the periodic roughness of

the pad surface was used to calculate the real contact area while the normal distribution of abrasive particle size was assumed to predict the number of active abrasives. To further take into account the effect of the pad surface roughness and the variation of asperity height on the material removal rate, Greenwood and Williamson's elastic contact model was commonly used to model the contact stress and the real area of pad/wafer contact in CMP [18, 19]. Bozkaya and Muftu [20] analyzed the contact interactions due to the two-body (pad-wafer) contact and the three-body (pad-particles-wafer) contact using contact mechanics and finite element (FE) modelling, and modelled the material removal rate by considering adhesive and abrasive wear mechanisms for CMP. Furthermore, Kim et al. [21, 22] developed the theoretical model based on contact mechanics and abrasive wear models to correlate pad surface topography and the material removal rate in CMP. According to the difference among processing conditions and the mechanisms between the CMP and CCBP, these models for CMP cannot be directly used for predicting the material removal rate in CCBP.

Despite intense theoretical and experimental research on bonnet polishing [23-25], there is still serous lack of fundamental understanding of extensive physical mechanisms in this process. As a result, the present paper presents a theoretical and experimental investigation of material removal characteristics in order to better understand and optimize the polishing process. A multi-scale model is built based on the study of contact mechanics, kinematics theory and wear mechanisms. Hence, a series of experiments have been undertaken to reassuringly validate the theoretical and simulated predictions.

2. Multi-scale theoretical modelling of material removal characteristics for computer controlled bonnet polishing

The material removal mechanism in CCBP involves multi-scale interaction between the pad, abrasive particles and the workpiece. Fig. 1 shows the flowchart of the theoretical modelling. The pressure and velocity distributions are determined based on the kinematics theory and contact mechanics at the macro scale, and the pad topography which affects the contact ratio and hence the material removal rate at the micro scale, and the micro- or nano-sized abrasive particles scratch the surface at the nano scale. In the coming section, the material removal characteristics is modeled step by step with the following assumptions: (1) The polishing bonnet is assumed to be a perfect sphere and much softer than the polished flat surface, hence, the polishing bonnet is elastically deformed while the polished surface remains flat in the contact area; (2) The polishing bonnet pressures the target flat surface is assumed to be a viscous sphere on a hard plane regardless of the contribution of slurry hydrodynamic pressure, pad asperities, contact-surface instability and pad-abrasive-workpiece contact;

(3) Material removal occurred in CCBP is assumed to be only related to the removal of material by plastic deformation caused by abrasive particles.

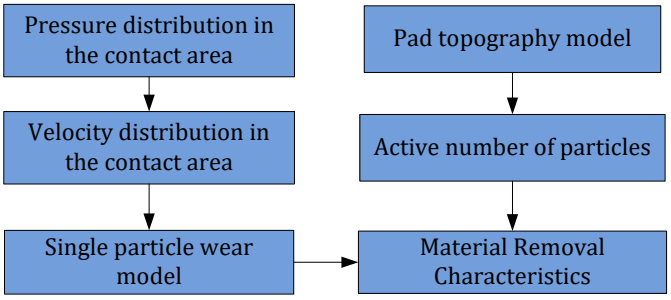

Fig.1 Flowchart of multi-scale theoretical modelling process for CCBP

2.1 Modelling of Surface Velocity Distribution

Fig. 2 shows the graphical illustration and detailed geometry in the polishing area by the polishing bonnet on flat surface. Where ω is angular velocity in rad/min, $\vec{\omega}=\frac{\pi S}{30}\{0,-\sin(\varphi),\cos(\varphi)\}$; φ is the inclination angle; S is angular velocity in rpm; O_b is the center of the bonnet; L is the axis of rotation of the bonnet; O_w is the center of polishing spot; d is the polishing depth in mm; R_b is the radius of the bonnet in mm; O_r is the swing center of point P and can be expressed as (0, y_0, $-y_0\cot\varphi$); P is any point in polishing contact area and can be expressed as ($(R_b-d)\tan\alpha\sin\theta$, $(R_b-d)\tan\alpha\cos\theta$, $-(R_b-d)$), $0\le\alpha\le\arccos\left(\frac{(R_b-d)}{R_b}\right)$, $0\le\theta\le2\pi$. Hence, the vector of $\overrightarrow{O_bO_r}$ and $\overrightarrow{O_rp}$ can be represented as

$$\overrightarrow{O_bO_r}=\{0,y_0,-y_0\cot\varphi\} \tag{1}$$

$$\overrightarrow{O_rp}=\{(R_b-d)\tan\alpha\sin\theta,(R_b-d)\tan\alpha\cos\theta-y_0,-(R_b-d)+y_0\cot\varphi\} \tag{2}$$

Since $\overrightarrow{O_bO_r}\perp\overrightarrow{O_rp}$, the solution of y_0 can be expressed as

$$y_0=\frac{(R_b-d)(\tan\alpha\cos\theta+\cot\varphi)}{1+(\cot\varphi)^2} \tag{3}$$

Therefore, the vector of $\overrightarrow{O_rp}$ can be written as

$$\overrightarrow{O_rp}=\{U,V,W\} \tag{4}$$

where $U=(R_b-d)\tan\alpha\sin\theta$; $V=(R_b-d)\tan\alpha\cos\theta-\frac{(R_b-d)(\tan\alpha\cos\theta+\cot\varphi)}{1+(\cot\varphi)^2}$;

$$W = -(R_b - d) + \frac{(R_b - d)(\tan\alpha\cos\theta + \cot\varphi)}{1 + (\cot\varphi)^2}\cot\varphi .$$

The velocity vector $\vec{v_p}$ at point P can be obtained by using vector operation (cross product):

$$\vec{v_p} = \vec{\omega} \times \vec{O_r p} = \frac{\pi S}{30}\left[-(V\cos\varphi + W\sin\varphi)\vec{i} + U\cos\varphi\,\vec{j} + U\sin\varphi\,\vec{k}\right] \tag{5}$$

Therefore, for polishing a flat surface, the relative velocity V_r at the point P is

$$V_r = \frac{\pi S}{30}\sqrt{(V\cos\varphi + W\sin\varphi)^2 + U^2(\cos\varphi)^2} \tag{6}$$

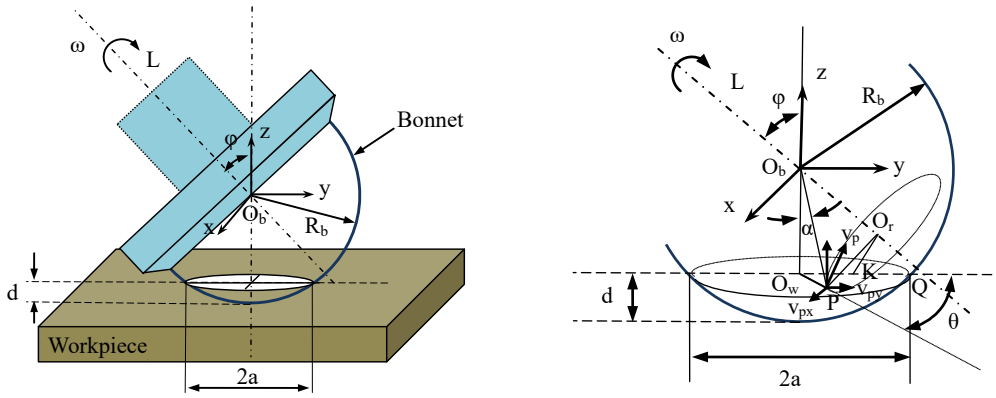

(a) (b)

Fig. 2 (a) Graphical illustration and (b) detailed geometry in the polishing area by the polishing bonnet on flat surface

2.2 Modelling of Pressure Distribution

Since the plasticity index for a soft polymer has only about one tenth of the value for metal, the contact between a polymer and a metal is almost completely elastic, except against very rough surfaces [26]. When an elastic sphere slides over a flat surface with the abrasive slurry, the pressure distribution in the contact area between the polishing pad and workpiece and the surface deformations of the polishing bonnet cannot be calculated independently by the Hertz's theory. In this paper, considering the strong time-dependence of mechanical properties of polymers, the polishing pad pressured the target flat surface was assumed to be a viscous sphere on a hard plane regardless of the contribution of slurry hydrodynamic pressure, pad asperities, contact-surface instability and pad-abrasive-workpiece contact. According to Brilliantov and Poschel [27], when the deformation of a sphere is rather small $d / R_b << 1$, the rolling velocity is much less than the sound speed in the sphere material and the characteristic time is much larger than the dissipative relaxation time of the material. The total stress

σ_{ij} is a sum of the elastic part of the stress tensor σ_{ij}^{el} and the dissipative part of the stress tensor σ_{ij}^{dis} (see Fig. 3).

$$\sigma_{ij}^{el} = E_1(\varepsilon_{ij} - \frac{1}{3}\delta_{ij}\varepsilon_{kk}) + E_2\varepsilon_{kk}\delta_{ij} \tag{7}$$

$$\sigma_{ij}^{dis} = \eta_1(\dot{\varepsilon}_{ij} - \frac{1}{3}\delta_{ij}\dot{\varepsilon}_{kk}) + \eta_2\dot{\varepsilon}_{kk}\delta_{ij} \tag{8}$$

where ε_{ij} and $\dot{\varepsilon}_{ij}$ denote the strain and strain rates, respectively. $E_1 = Y/(1+\nu)$ and $E_2 = Y/3(1-2\nu)$ denote the elastic material constants with Y and ν being the Young modulus and the Poisson ratio, respectively. η_1 and η_2 are the coefficients of viscosity, related to shear and bulk deformation respectively. δ_{ij} is the Kronecker symbol. Subscripts in Eqs. (7) and (8) follow the Einstein notation. From the Eqs. (7) and (8), the diagonal component of the stress tensor can be expressed as

$$\sigma_{zz}^{el} = E_1(\varepsilon_{33} - \frac{1}{3}\delta_{33}\varepsilon_{kk}) + E_2\varepsilon_{kk}\delta_{33} = E_1\frac{\partial u_z}{\partial z} + \left(E_2 - \frac{E_1}{3}\right)\left(\frac{\partial u_x}{\partial x} + \frac{\partial u_y}{\partial y} + \frac{\partial u_z}{\partial z}\right) \tag{9}$$

$$\sigma_{zz}^{dis} = \eta_1(\dot{\varepsilon}_{33} - \frac{1}{3}\delta_{33}\dot{\varepsilon}_{kk}) + \eta_2\dot{\varepsilon}_{kk}\delta_{33} = \eta_1\frac{\partial \dot{u}_z}{\partial z} + \left(\eta_2 - \frac{\eta_1}{3}\right)\left(\frac{\partial \dot{u}_x}{\partial x} + \frac{\partial \dot{u}_y}{\partial y} + \frac{\partial \dot{u}_z}{\partial z}\right) \tag{10}$$

where u_x, u_y and u_z denote the x- ,y- and z- direction displacement field of the classic Hertz contact problem. $\dot{u}_x$, $\dot{u}_y$ and $\dot{u}_z$ denote the time derivative of the displacement field in x-, y- and z-direction, respectively. σ_{zz}^{el} has the known solution for the Hertz contact problem [28].

$$\sigma_{zz}^{el} = E_1\frac{\partial u_z}{\partial z} + \left(E_2 - \frac{E_1}{3}\right)\left(\frac{\partial u_x}{\partial x} + \frac{\partial u_y}{\partial y} + \frac{\partial u_z}{\partial z}\right) = p_0\left(1 - \frac{x^2}{a^2} - \frac{y^2}{a^2}\right)^{1/2} \tag{11}$$

where $a = \sqrt{dR_b}$ denotes the radius of contact area and $p_0 = 3F_N/(2\pi a^2)$ denotes the maximum contact pressure, F_N is the total elastic force, acting by the surface (in normal direction) on the polishing pad:

$$F_N = \frac{2}{3}\frac{Y}{(1-\nu^2)}R_b^{1/2}d^{3/2} \tag{12}$$

$\sigma_{zz}^{el}(E_1 \leftrightarrow \eta_1; E_2 \leftrightarrow \eta_2)$ was derived by Brilliantov and Poschel [27] and Brilliantov et al. [29] using a technique of coordinate's transformation. But Zheng et al. [30] noted inappropriate equality in their derivation and obtained $\sigma_{zz}^{el}(E_1 \leftrightarrow \eta_1; E_2 \leftrightarrow \eta_2)$ directly based on the principles of contact mechanics [31] as follows,

$$\sigma_{zz}^{el}(E_1 \leftrightarrow \eta_1; E_2 \leftrightarrow \eta_2) = -\frac{(1-2\nu)(1+\nu)}{Y}(2\eta_2 + \eta_1/3)P_0\left(1 - \frac{x^2}{a^2} - \frac{y^2}{a^2}\right)^{1/2} \tag{13}$$

Kinematic equation is used to describe the displacement velocity distribution,

$$\dot{\vec{u}}(x,y,z)=\left(\vec{\Omega}\cdot\vec{r}\times\vec{\nabla}\right)\vec{u}(x,y,z)=-\omega\cos\varphi(z\partial x-x\partial z)\vec{u}(x,y,z)+\omega\sin\varphi(x\partial y-y\partial x)\vec{u}(x,y,z) \quad (14)$$

where $\vec{\Omega}=\{0,-\omega\cos\varphi,\omega\sin\varphi\}$, ω is the angular velocity, φ is the inclined angle. Eq. (14) coupled with the definitions of the elastic part and dissipative part of the stress tensor [27, 28] is used to obtain the dissipative part of the stress tensor as follows

$$\begin{aligned}\sigma_{zz}^{dis}&=\omega\sin\varphi(x\partial y-y\partial x)\sigma_{zz}^{el}(E_1\leftrightarrow\eta_1;E_2\leftrightarrow\eta_2)-\omega\cos\varphi(z\partial x-x\partial z)\sigma_{zz}^{el}(E_1\leftrightarrow\eta_1;E_2\leftrightarrow\eta_2)+\\&(\eta_2-\eta_1/3)\omega\cos\varphi\partial z u_x-(\eta_2+2\eta_1/3)\omega\cos\varphi\partial x u_z+(\eta_2-\eta_1/3)\omega\sin\varphi\partial y u_x-(\eta_2-\eta_1/3)\omega\sin\varphi\partial x u_y\end{aligned} \quad (15)$$

where $\partial x=\frac{\partial}{\partial x}$, $\partial y=\frac{\partial}{\partial y}$, $\partial z=\frac{\partial}{\partial z}$; $\vec{u}(x,y,z)=(u_x,u_y,u_z)$ and $E_1\leftrightarrow\eta_1,E_2\leftrightarrow\eta_2$, etc. u_z is the surface displacements in the normal and radial direction and can be expressed as:

$$u_z=(1-v^2)\pi p_0(2a^2-x^2-y^2)/(4Ya) \quad (16)$$

Similar to the reference [27], some terms can be omitted by calculation the relative magnitude. Eq. (15) can be casted as

$$\sigma_{zz}^{dis}=-\frac{(1-2v)(1+v)}{Y}\cdot\frac{\omega\cos\varphi(2\eta_2+\eta_1/3)p_0xz}{a^2}\cdot\left(1-\frac{x^2}{a^2}-\frac{y^2}{a^2}\right)^{-1/2}+\frac{(1-v)^2}{Y}\cdot\frac{\omega\cos\varphi(2\eta_2+\eta_1/3)\pi p_0x}{2a} \quad (17)$$

As a result, the pressure distribution at the polishing contact area can be expressed by

$$\begin{aligned}P(x,y)=\sigma_{zz}^{el}+\sigma_{zz}^{dis}&=p_0\left(1-\frac{x^2}{a^2}-\frac{y^2}{a^2}\right)^{1/2}-\frac{(1-2v)(1+v)}{Y}\\&\cdot\frac{\omega\cos\varphi(2\eta_2+\eta_1/3)p_0xz}{a^2}\cdot\left(1-\frac{x^2}{a^2}-\frac{y^2}{a^2}\right)^{-1/2}+\frac{(1-v)^2}{Y}\cdot\frac{\omega\cos\varphi(2\eta_2+\eta_1/3)\pi p_0x}{2a}\end{aligned} \quad (18)$$

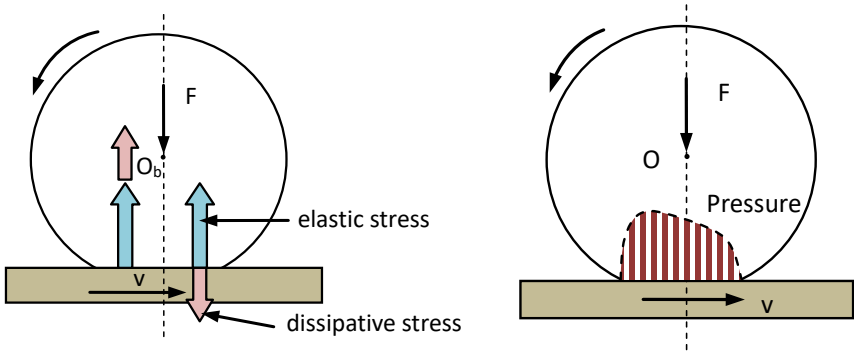

(a) (b)

Fig.3 Sketch of pressure distribution for the rolling bonnet

2.3 Single Particle Wear Model

The yield load, W_y, is calculated as a function of the particle radius, R_p, and the mechanical properties of the workpiece based on Hertzian analysis and the Tresca criterion [32]:

$$W_y = \frac{\pi^3}{48}\frac{H_w^3}{E_w^2}R_p^2 \tag{19}$$

where E_w and H_w are the young's modulus and hardness of the workpiece, respectively. As can be seen in Fig. 4(a), an abrasive particle, assumed to be spherical and rigid with the radius of R_p, is dragged across the surface in plastic contact which flows under an indentation pressure p_n. It forms a groove on the target surface and some proportion of the material is removed by the particle. Since the depth of indentation, δ_p, is much smaller than the radius of the abrasive, the depth is related to the radius of the projected circle of contact, a_p, by

$$\delta_p = \frac{a_p^2}{2R_p} \tag{20}$$

For a polishing process, the particle is moving with relative velocity, V_r, and hence in contact only over its front surface (see Fig. 4(c)),

$$W_p = \frac{\pi a_p^2 p_n}{2} = \pi\delta_p R_p p_n \approx \pi\delta_p R_p H_w \tag{21}$$

Since the abrasive penetration into the target surface is at the nanometer scale, the mechanism of plastic deformation may involves multi-phase transformations without introducing dislocations, planar defects or micro-cracks [33]. In this study, a fraction η of the material displaced from the groove is actually removed as wear debris, then the volume removed by this abrasive particle per unit time is

$$Vol_p' = \eta\delta_p a_p V_r = \frac{\sqrt{2}}{\pi^{3/2}}\frac{\eta V_r}{R_p}\left(\frac{W_p}{H_w}\right)^{3/2} \tag{22}$$

As can be seen in Fig. 4(b), an abrasive particle was idealized as a cone of semiangle α. The depth of indentation, δ_p, is related to the radius of the projected circle of contact, a_p, by

$$a_p = \delta_p \tan\alpha \tag{23}$$

For the cone particle, Eq. (21) can be rewritten as

$$W_p = \frac{\pi a_p^2 p_n}{2} = \frac{\pi\delta_p^2(\tan\theta)^2 p_n}{2} \approx \frac{\pi\delta_p^2(\tan\theta)^2 H_w}{2} \tag{24}$$

Hence, the volume of wear debris produced by the cone particle per unit time is expressed by

$$Vol_p'' = \eta\delta_p a_p V_r = \eta\delta_p^2 \tan\alpha V_r = \frac{2\eta W_p V_r}{\pi H_w \tan\alpha} \tag{25}$$

From the above analysis, the wear rate of a single abrasive particle depends heavily on the particle's shape. However, the angularity of abrasive particles is difficult to be defined and this is mainly due to the difficulty of identifying and quantifying the features of a complex three-dimensional shape causing its abrasivity. Since angular particles cause more material removal than spherical particles [26], cone particles are commonly used in the polishing process.

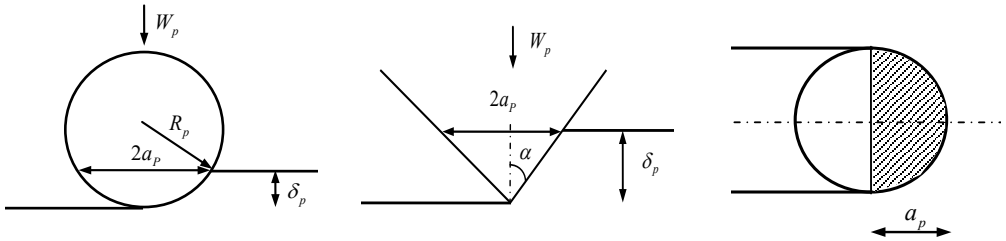

(a) (b) (c)

Fig.4 Geometry of contact between an abrasive particle and a surface: (a) and (b) in elevation; (c) in plan view

2.4 Active Number of abrasive particles

The slurry particles involved in material removal are those that are embed in the surface of the compliant polishing pad and are dragged across the polished surface by the relative velocity between the two surfaces, and the active number of these particles is generally related to the particle size distribution, the hydrodynamics condition between the polishing pad and the workpiece as well as the surface topography of the polishing pad and target surface. To simplify the theoretical modelling, the pad-particle-workpiece contact is assumed to be solid-solid contact neglecting the effects of the fluid flow, and the particle size is assumed to be a constant. According to Luo and Dornfield [17], in this paper, the abrasive particles engaged in two-body abrasion are regarded as only agents of effective material removal. The effective contact area between the polishing pad and the entrained particle is approximately equal to πR_p^2, and hence the force applied on an abrasive, W_p, can be expressed by

$$W_p = \pi R_p^2 P(x,y) \tag{26}$$

Since the polishing pad tends to be deteriorated in the polishing process [34], the modelling of the surface topography of the polishing pad is very hard. Statistical theories were used to model the surface topography of polishing pad assessing by the pad asperity radius R_a and the standard deviation of asperity heights σ_z [35, 36]. For relatively soft pad and low abrasive concentration, the active number of abrasive particles tends to be proportional to the real contact area and the slurry concentration [37, 38]. As a result, the active number of abrasive particles can be expressed by

$$N_{ac} = K_{ac} \frac{V_c t}{R_p^2} \left(\frac{R_a}{\sigma_z} \right)^{1/2} \tag{27}$$

where K_{ac} is the coefficient related to the particle size distribution and the hydrodynamics condition, t is the polishing time, V_c is the volume fraction, R_a is the radius of the pad asperities, and σ_z is the standard deviation of asperity heights. As a result, the material removal rate can be predicted by

$$Vol_{mmr} = N_{ac} Vol_p{}'' = \frac{2\eta K_{ac} V_c t V_r(x,y) P(x,y)}{H_w \tan\alpha} \left(\frac{R_a}{\sigma_z} \right)^{1/2} \tag{28}$$

Therefore, model of the material removal characteristics developed in this study, relating to the

slurry concentration, particle shape, polishing depth, tool size, head speed, polishing time, pad topography and hardness of polishing pad and polished surface, reveals some insights into the contact mechanics and the wear mechanisms of the CCBP process. It suggests that the material removal rate is proportional to the slurry concentration, the polishing time, the velocity and the pressure distribution, and inversely proportional to the hardness of the polished surface. The velocity distribution is proportional to the head speed and the pressure distribution is proportional to the applied load and hence this proportional relation is agree well with the Preston's equation. Moreover, the model reveals that both of the polishing depth (the down force) and rotational speed have obvious effects on the pressure distribution in the polishing area for bonnet polishing. Hence the calculation of the pressure in the model taking into account of the hardness of the polishing pad can explain the asymmetric pressure distribution in X- cross-section due to the strong time-dependence of mechanical properties of the polishing bonnet. According to the proposed model, larger radius of the pad asperities and smaller standard deviation of asperity heights represents higher material removal rate.

3. Experimental Verification

The multi-scale theoretical model for CCBP was verified through a series of simulation and polishing experiments. A simulation program was purposely developed by the authors for the implementation of the model using the MATLAB software package. Fig.5 shows the Zeeko IRP 200 ultra-precision freeform polishing machine used in the experiments. In this study, a bonnet with a radius of 20 mm was assembled on the main spindle, while the workpiece made of steel (S136) was fixed on the C axis. All samples were polished by a LP-66 (Cerium oxide D'27) polished pad with a slurry comprising 2.066 vol. % of Al_2O_3 abrasives with an average size of 13.12 μm during the constant machining time of 60 s. A series of simulations were constructed under the same conditions that were adopted for experiments as shown in Table 1, while the other coefficients used in the simulations are shown in Table 2.

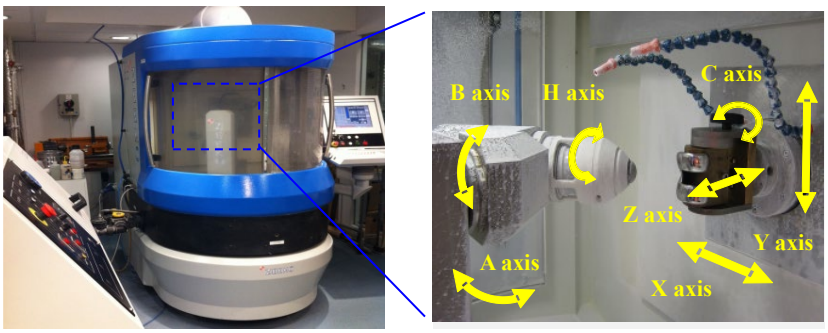

Fig.5 Zeeko IRP200 Ultra-precision freeform polishing machine

Table 1: Process parameters of polishing experiments

Sample No.	Tool pressure	Tool offset	Head speed	*Precess* angle
A1	1.2 bar	0.1 mm	1200 rpm	10°
A2	1.2 bar	0.1 mm	1200 rpm	15°
A3	1.2 bar	0.1 mm	1200 rpm	20°
B1	1.2 bar	0.1 mm	900 rpm	15°
B2	1.2 bar	0.1 mm	1200 rpm	15°
B3	1.2 bar	0.1 mm	1500 rpm	15°
C1	1.2 bar	0.08 mm	1200 rpm	15°
C2	1.2 bar	0.12 mm	1200 rpm	15°
C3	1.2 bar	0.16 mm	1200 rpm	15°

Table 2: Parameters used in the present simulation

Variable	Symbol	Base value
Young's modulus	Y	2 Mpa [30]
Poisson's ratio	ν	0.3 [30]
Viscosity coefficient	η_1	2×10-4 Mpa·s [30]
Viscosity coefficient	η_2	0 Mpa·s [30]
Semiangle of cone particle	α	45°
Hardness of workpiece	H_w	509 Mpa
Radius of pad asperities	R_a	23.5 μm [21]
Standard deviation	σ_z	4.4 μm [21]

Fig.6(a) shows the experimental data of polished spot measured by a Zygo Nexview 3D Optical Surface Profiler, while Fig.6(b) shows the predicted 3D topography of the material removal characteristics for the case of B3. It was found that the predicted result of the theoretical model shows a good correlation in surface shape with the experimental data. The cross-section curve of the X-Z profile and Y-Z profile of the measured experimental data passing the deepest point were used to verify the theoretical model as shown in Fig.6 (c) and 6(d), respectively. It turned out that the simulated result by the theoretical model agreed reasonably well with the measured data. It is interesting to note that the width of the X-Z profile was significantly larger than that for the Y-Z profile and hence the real contact area was not a circle. This may be due to the deformation of the polishing bonnet and/or the swing of the main spindle. Due to the new calculation method for pressure distribution, the theoretical model was found to be able to explain the asymmetry of the X-Z profile and Y-Z profile of the polished spot. This infers that the contact mechanics and kinetics theory proposed in this study can provide an explanation for the polishing mechanisms in bonnet polishing.

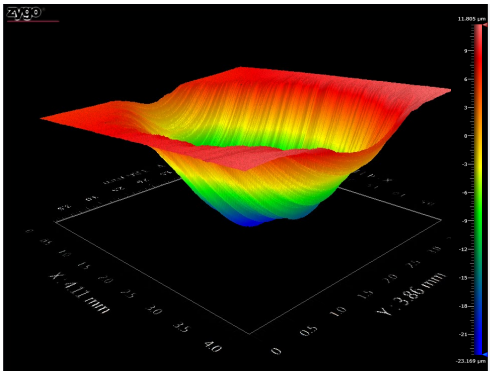

(a) Measured 3D topography data

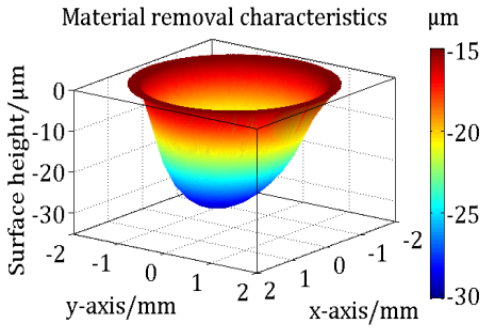

(b) Predicted 3D influence function

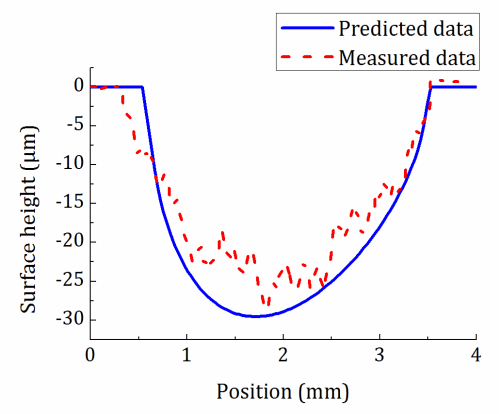

(c) X-Z profile of TIF

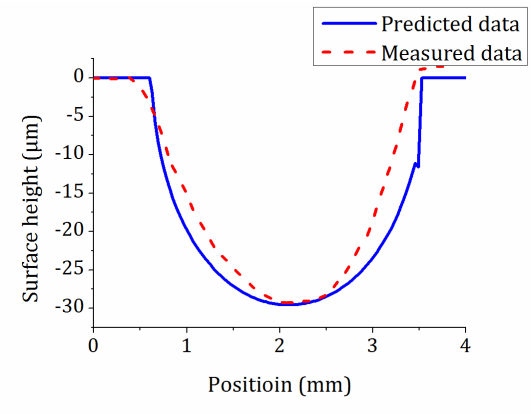

(d) Y-Z profile of TIF

Fig.6 Results of the simulation and experiment in terms of 3D topography, X-Z profile and Y-Z profile (for the case of B3)

To evaluate the accuracy of the predictions under different polishing conditions, predicted data by Preston equation based Hertz contact theory [15] were used to compare with simulated results of the developed theoretical model. These simulation results and measurements were shown in Fig. 7. To describe the two approaches clearly and concisely, Preston equation with Hertz contact mechanics and the developed multi-scale material removal model were temporarily named as Preston model and multi-scale model in this paper respectively. Fig.7(a) shows that the material removal amount increased with an increase of the *precess* angle. This is due to the fact that a higher *precess* angle means a higher velocity distribution in the contact area and hence a higher material removal rate is obtained. It can be explained reasonably well by the developed multi-scale model. Fig.7(b) shows that the volumetric material removal rate increased linearly with increasing head speed and this can be predicted well by the multi-scale model. Both experimental and predicted results (see Fig.7(c)) show that the volumetric material removal increased as the tool offset was increased. This can be explained by a larger tool offset presenting a larger contact area and higher contact pressure and hence a higher material removal rate. Moreover, it is interesting to note that the predicted results of the multi-scale model are larger than

the simulated results of Preston model with Hertz contact mechanics. This can be explained by the pressure distribution of new approach which takes into account of the strong time-dependence of mechanical properties of polishing bonnet. Hence, the accuracy of the new approach is better than that of Preston model with Hertz contact mechanics, while the multi-scale material removal model captures much of the basic physics of the polishing process.

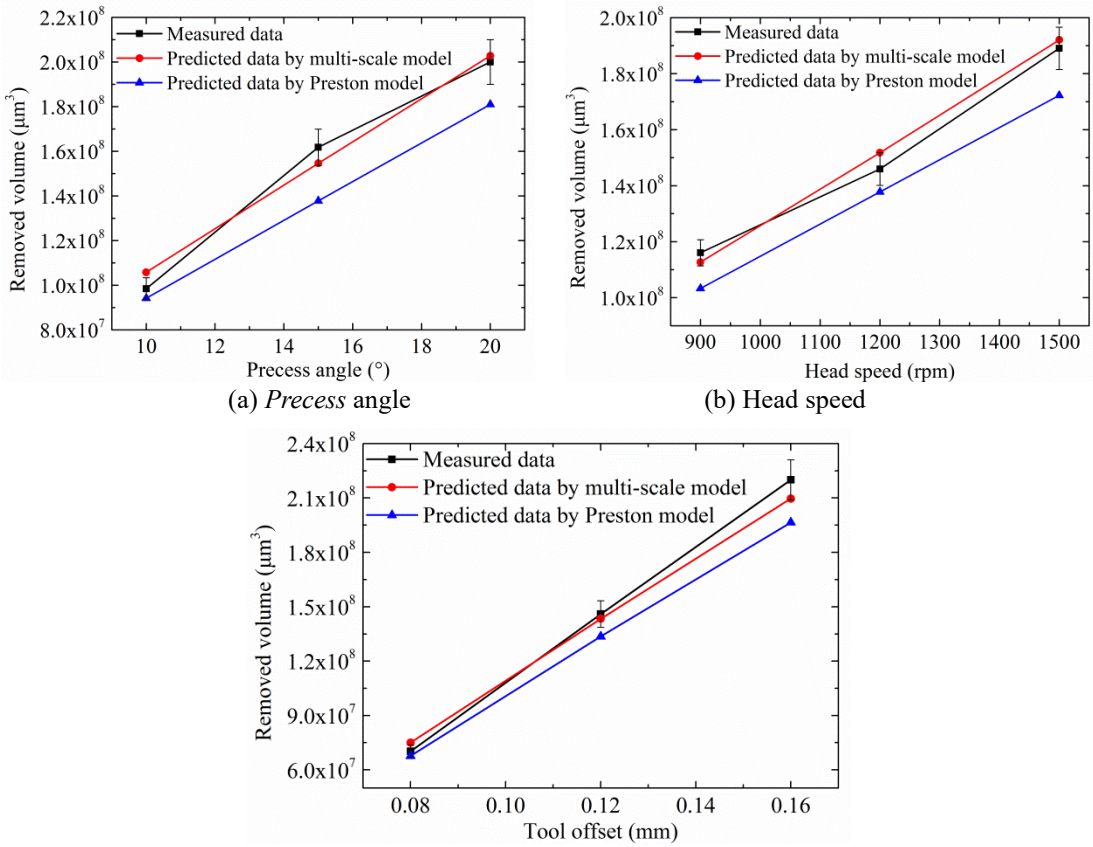

(a) *Precess* angle (b) Head speed

(c) Tool offset

Fig.7 Comparison of measured data and simulation results under different (a) *precess* angles, (b) head speeds and (c) tool offsets

In the practical polishing experiments, the material removal amount may not be proportional to the pressure value in some positions of the polished spot under some polishing conditions [16]. To investigate this phenomenon, a seires of spot tests were conducted by carrying out polishing tests at one place, while surface tests were also performed by translating the polishing tool along flat surfaces. In the spot tests, three samples made of steel (S136) were prepared by deterministic micro-grinding of Moore Nanotech® 450UPL and they were then polished by a Zeeko IRP 200 ultra-precision freeform polishing machine. Experiments were conducted under different polishing depths of 0.1 mm, 0.3 mm and 0.5 mm, while other parameters are kept the same as the polishing conditions for sample C2. The

polished samples were measured by a Zygo Nexview 3D Optical Surface Profiler and HITACHI TM3000 Tabletop Scanning Electron Microscope, and the measured results were shown in Table 3. Results show that the material removal amount was proportional to the pressure distribution for a tool offset of 0.1mm and 0.3 mm, while little material was removed in the position with the highest pressure for a tool offset of 0.5 mm. This may be caused by the deformation of the polishing bonnet when large tool offset is used in bonnet polishing. Another factor that should be considered is that when polishing the surface at a large polishing depth, the pressure is highest at the centre of the contact area, and then the slurry film is broken up. This means that the slurry is hardly entrapped in the contact area and the material is mainly removed by the polishing pad and hence the amount of material removal is significantly small. It is interesting to note that micro- and/or nano-scale scratches are produced on the surface at the centre of the contact area. This infers that the surface is easily scratched by the polishing pad when the pressure is high and the slurry film is broken up.

Table 3: Experimental results of spot tests for three different polishing depth

Sample No.	Zygo photographs	SEM photographs (Center area)
D1 (Polishing depth: 0.1 mm)	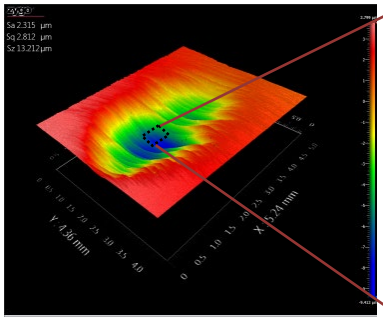	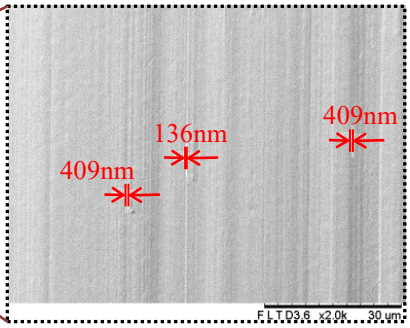
D2 (Polishing depth: 0.3 mm)	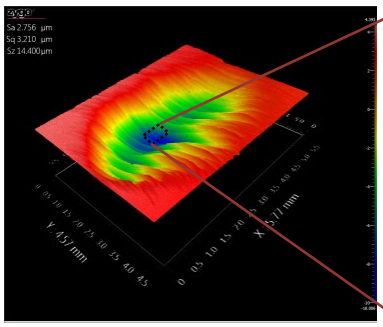	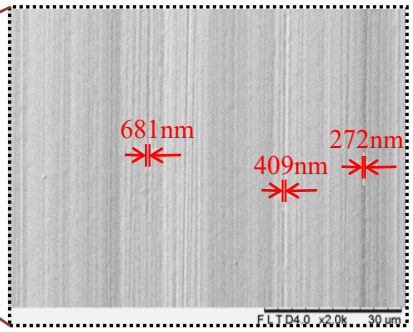
D3 (Polishing depth: 0.5 mm)	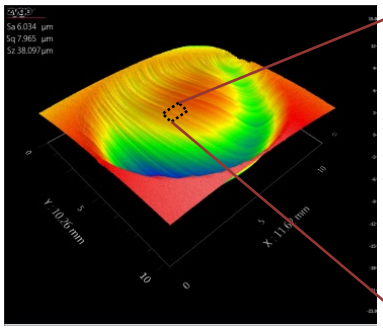	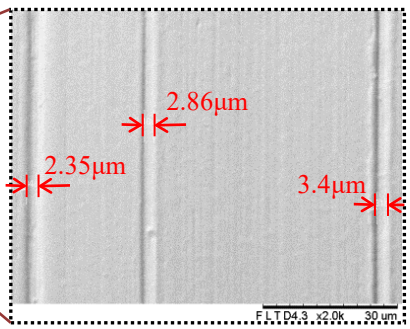

In the surface tests, a flat sample made of steel (S136) is divided into four areas including: (i) non-polish area which is studied as the surface before polishing; (ii) polishing area which is polished by using the polishing depth of 0.1 mm; (iii) polishing area which is polished by using the polishing depth of 0.3 mm; (iv) polishing area which is polished by using the polishing depth of 0.5 mm. Raster mode with the feed rate of 50 mm/min and Al_2O_3 abrasives with an average size of 3.22 μm were used in the surface tests and other parameters are the same as the polishing conditions for sample C2. Fig.8 shows experimental data observed by a Zygo Nexview 3D Optical Surface Profiler in the surface tests. It is interesting to note that better surface roughness is obtained under a lager polishing depth between 0 mm and 0.3 mm. The surface roughness of the surface polished by using the polishing depth of 0.5 mm is even worse than that of the non-polishing surface.

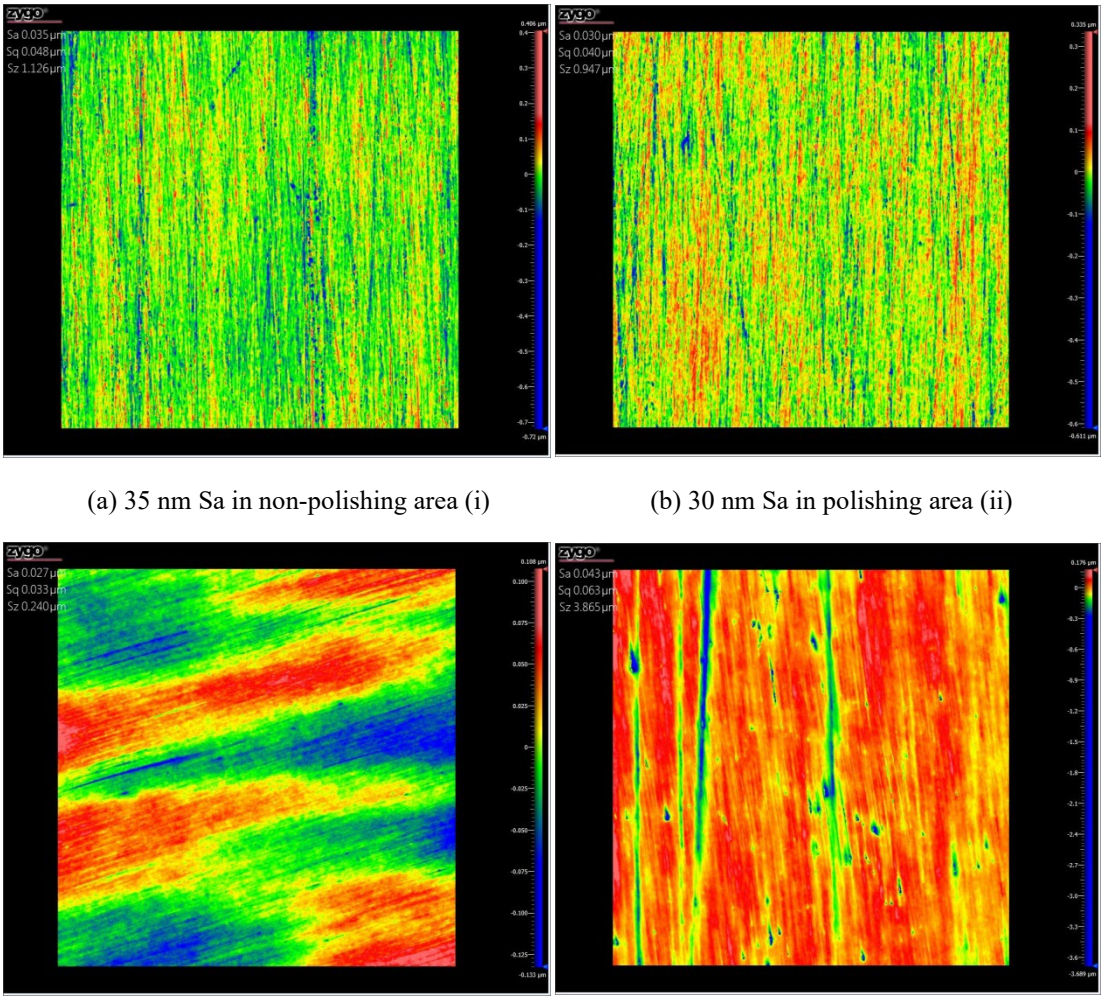

(a) 35 nm Sa in non-polishing area (i)

(b) 30 nm Sa in polishing area (ii)

(c) 27 nm Sa in polishing area (iii)

(d) 43 nm Sa in polishing area (iv)

Fig.8 Experimental data observed by a Zygo Nexview 3D Optical Surface Profiler in the surface tests

Hence, there exists a critical polishing depth which if exceeded would lead to the breaking of the hydrodynamic lubrication condition which causes the pad scratching and/or deteriorates the surface finish. In other words, the tool offset in CCBP should be smaller than the critical polishing depth in order to ensure high surface quality with high polishing efficiency. The critical polishing depth is affected by tool pressure, pad topography, particle size and the material polishing pad material and polished surface in CCBP. On the whole, the multi-scale theoretical model for predicting the material removal characteristics in CCBP has been successfully developed and experimentally verified. It provides a better understanding of the effect of process parameters on computer-controlled bonnet polishing.

4. Conclusions

Due the complex machining mechanism, it is still difficult to model the material removal characteristics in computer controlled bonnet polishing (CCUP). This paper presents a theoretical and experimental study of the material removal characteristics in CCUP. The major findings are summarized as follows:

(1) A multi-scale theoretical model has been established for predicting and characterizing the materials removal characteristics in CCUP based on the study of contact mechanics, kinematics theory and wear mechanisms. Specifically, the pressure and velocity distributions are determined based on the kinematics theory and contact mechanics at the macro scale, and the pad topography which affects the contact ratio and hence the material removal rate at the micro scale, and the micro- or nano-sized abrasive particles scratch the surface at the nano scale. The model developed in this work captures much of the basic physics of the polishing process including the tool radius, polishing depth, head speed, *precess* angle, pad topography, polishing time, particle shape, slurry concentration and the mechanic property of pad and workpiece.

(2) The calculation of the pressure in the model taking into account of the strong time-dependence of mechanical properties of polishing bonnet reveals that both of the polishing depth (the down force) and rotational speed have obvious effects on the pressure distribution in the polishing area, and hence can explain the asymmetry of the material removal characteristics in X- cross-section.

(3) A series of spot tests as well as simulation experiments by the theoretical model were conducted. Experiments show that the theoretical model predicts well that the material removal amount increases with the increasing *precess* angle and tool offset, and depends linearly on the head speed. The

result reveals that the established theoretical model can be successfully used for predicting and better understanding the polishing process in CCUP.

(4) The results also suggest that there exists a critical polishing depth which if exceeded would lead to the breaking of the hydrodynamic lubrication condition in the high pressure area of polished spot which causes the pad scratching and/or deteriorates the surface finish.

Acknowledgement

The work described in this paper was fully supported by a grant from the Research Grants Council of the Government of the Hong Kong Special Administrative Region, China (Project No.: PolyU 5132/11E). The work was also supported by a PhD studentship (project code: RTC3) from The Hong Kong Polytechnic University.

References

[1] C.F. Cheung, H.F. Li, W.B. Lee, S. To, L.B. Kong, An integrated form characterization method for measuring ultra-precision freeform surfaces, Int J Mach Tool Manu, 47 (2007) 81-91.

[2] C.F. Cheung, L.B. Kong, M.J. Ren, D. Whitehouse, S. To, Generalized form characterization of ultra-precision freeform surfaces, Cirp Ann-Manuf Techn, 61 (2012) 527-530.

[3] Z.C. Cao, C.F. Cheung, Theoretical modelling and analysis of the material removal characteristics in fluid jet polishing, Int J Mech Sci, 89 (2014) 158-166.

[4] D.D. Walker, A.T.H. Beaucamp, D. Brooks, R. Freeman, A. King, G. McCavana, R. Morten, D. Riley, J. Simms, Novel CNC polishing process for control of form and texture on aspheric surfaces, Current Developments in Lens Design and Optical Engineering Iii, 4767 (2002) 99-105.

[5] D.D. Walker, R. Freeman, G. McCavana, R. Morton, D. Riley, J. Simms, D. Brooks, E.D. Kim, A. King, The Zeeko/UCL process for polishing large lenses and prisms, Large Lenses and Prism, 4411 (2002) 106-111.

[6] R.G. Bingham, D.D. Walker, D.H. Kim, D. Brooks, R. Freeman, D. Riley, A novel automated process for aspheric surfaces, Current Developments in Lens Design and Optical Systems Engineering, 4093 (2000) 445-450.

[7] F.W. Preston, The theory and design of plate glass polishing machines, J. Soc. Glass Technol., 11 (1927) 214-256.

[8] J.E. DeGroote, A.E. Marino, J.P. Wilson, A.L. Bishop, J.C. Lambropoulos, S.D. Jacobs, Removal rate model for magnetorheological finishing of glass, Appl Optics, 46 (2007) 7927-7941.

[9] R.E. Wagner, R.R. Shannon, Fabrication of Aspherics Using a Mathematical-Model for Material Removal, Appl Optics, 13 (1974) 1683-1689.

[10] T.I. Suratwala, M.D. Feit, W.A. Steele, Toward Deterministic Material Removal and Surface Figure During Fused Silica Pad Polishing, J Am Ceram Soc, 93 (2010) 1326-1340.

[11] C.F. Cheung, L.B. Kong, L.T. Ho, S. To, Modelling and simulation of structure surface generation

using computer controlled ultra-precision polishing, Precis Eng, 35 (2011) 574-590.
[12] H. Li, D. Walker, G. Yu, W. Zhang, Modeling and validation of polishing tool influence functions for manufacturing segments for an extremely large telescope, Appl Opt, 52 (2013) 5781-5787.
[13] H.Y. Li, G.Y. Yu, D. Walker, R. Evans, Modelling and measurement of polishing tool influence functions for edge control, J Eur Opt Soc-Rapid, 6 (2011).
[14] C. Wang, Z. Wang, X. Yang, Z. Sun, Y. Peng, Y. Guo, Q. Xu, Modeling of the static tool influence function of bonnet polishing based on FEA, Int J Adv Manuf Tech, 74 (2014) 341-349.
[15] C. Bouvier, Investigation of polishing algorithms and removal processes for a deterministic subaperture polisher, (2007).
[16] S.Y. Zeng, L. Blunt, Experimental investigation and analytical modelling of the effects of process parameters on material removal rate for bonnet polishing of cobalt chrome alloy, Precis Eng, 38 (2014) 348-355.
[17] J.F. Luo, D.A. Dornfeld, Material removal mechanism in chemical mechanical polishing: Theory and modeling, Ieee T Semiconduct M, 14 (2001) 112-133.
[18] J. Seok, C.P. Sukam, A.T. Kim, J.A. Tichy, T.S. Cale, Multiscale material removal modeling of chemical mechanical polishing, Wear, 254 (2003) 307-320.
[19] Y. Zhao, L. Chang, A micro-contact and wear model for chemical–mechanical polishing of silicon wafers, Wear, 252 (2002) 220-226.
[20] D. Bozkaya, S. Muftu, A Material Removal Model for CMP Based on the Contact Mechanics of Pad, Abrasives, and Wafer, J Electrochem Soc, 156 (2009) H890-H902.
[21] S. Kim, N. Saka, J.H. Chun, The Role of Pad Topography in Chemical-Mechanical Polishing, Ieee T Semiconduct M, 27 (2014) 431-442.
[22] S. Kim, N. Saka, J.H. Chun, S.H. Shin, Modeling and mitigation of pad scratching in chemical-mechanical polishing, Cirp Ann-Manuf Techn, 62 (2013) 307-310.
[23] A. Beaucamp, Y. Namba, Super-smooth finishing of diamond turned hard X-ray molding dies by combined fluid jet and bonnet polishing, Cirp Ann-Manuf Techn, 62 (2013) 315-318.
[24] A. Beaucamp, Y. Namba, P. Charlton, Corrective finishing of extreme ultraviolet photomask blanks by precessed bonnet polisher, Appl Opt, 53 (2014) 3075-3080.
[25] D. Walker, G.Y. Yu, H.Y. Li, W. Messelink, R. Evans, A. Beaucamp, Edges in CNC polishing: from mirror-segments towards semiconductors, paper 1: edges on processing the global surface, Opt Express, 20 (2012) 19787-19798.
[26] I.M. Hutchings, Tribology: friction and wear of engineering materials, (1992).
[27] N.V. Brilliantov, T. Poschel, Rolling friction of a viscous sphere on a hard plane, Europhys Lett, 42 (1998) 511-516.
[28] L.D. Landau, E.M. Lifshitz, Theory of Elasticity, Pergamon Press, 1959.
[29] N.V. Brilliantov, F. Spahn, J.M. Hertzsch, T. Poschel, Model for collisions in granular gases, Physical review. E, Statistical physics, plasmas, fluids, and related interdisciplinary topics, 53 (1996) 5382-5392.

[30] Q.J. Zheng, H.P. Zhu, A.B. Yu, Finite element analysis of the rolling friction of a viscous particle on a rigid plane, Powder Technol, 207 (2011) 401-406.
[31] K.L. Johnson, K.L. Johnson, Contact mechanics, Cambridge university press, 1987.
[32] N. Saka, T. Eusner, J.H. Chun, Nano-scale scratching in chemical–mechanical polishing, CIRP Annals - Manufacturing Technology, 57 (2008) 341-344.
[33] L. Zhang, I. Zarudi, Towards a deeper understanding of plastic deformation in mono-crystalline silicon, Int J Mech Sci, 43 (2001) 1985-1996.
[34] L.C. Zhang, A.Q. Biddut, Y.M. Ali, Dependence of pad performance on its texture in polishing mono-crystalline silicon wafers, Int J Mech Sci, 52 (2010) 657-662.
[35] S. Kim, N. Saka, J.H. Chun, The Effect of Pad-asperity Curvature on Material Removal Rate in Chemical-mechanical Polishing, Procedia CIRP, 14 (2014) 42-47.
[36] J. Greenwood, J. Williamson, Contact of nominally flat surfaces, Proceedings of the Royal Society of London. Series A. Mathematical and Physical Sciences, 295 (1966) 300-319.
[37] G.H. Fu, A. Chandra, S. Guha, G. Subhash, A plasticity-based model of material removal in chemical-mechanical polishing (CMP), Ieee T Semiconduct M, 14 (2001) 406-417.
[38] J.F. Luo, D.A. Dornfeld, Effects of abrasive size distribution in chemical mechanical planarization: Modeling and verification, Ieee T Semiconduct M, 16 (2003) 469-476.

List of Figure Caption